Electronic Supplementary Information for

Experimental evidence for large negative electron affinity from scandium-terminated diamond

Ramiz Zulkharnay* and Paul W. May

School of Chemistry, University of Bristol, Cantock's Close, Bristol BS8 1TS, United Kingdom.

* Corresponding author: E-mail: ramiz.zulkharnay@bristol.ac.uk

S-1. AFM measurements

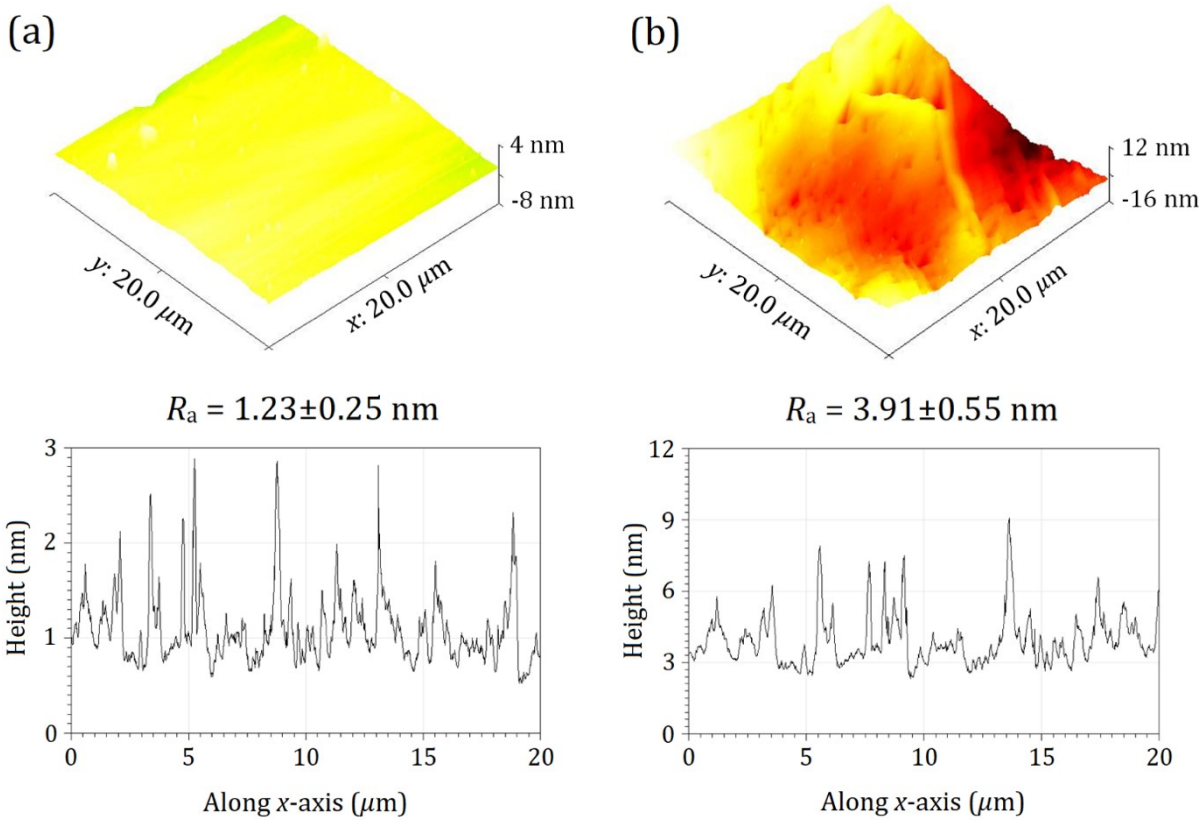

Fig. S1. Atomic Force Microscopy (AFM) 3D maps with corresponding surface roughness plots for as-received single-crystal (a) (100) and (b) (111) samples, after acid washing procedures.

S-2. SPA-LEED study

S-2.1 H-terminated diamond (100) and (111) surfaces

Hydrogenated diamond (100) has two orthogonal spots, which are rotated by 90° with respect to each other, possessing two commensurate (2 × 1) or (1 × 2) reconstructions as given in Fig. S2(a). In contrast, for H-terminated (111) diamond, there is only a single domain of (1 × 1) topology related by 120° rotation on a hexagonal lattice (Fig. S2(b)). These two LEED patterns supported by sharp intensities of characteristic domains show 'ideal' and thermodynamically favorable structures for both hydrogenated surfaces.

For both hydrogenated surfaces, experimentally obtained data were supported by the *LEEDpat* simulation (Fig. S2(c) and (d) and Fig. S3(c) and (d)) and DFT modelling (Fig. S3(a) and (b)) to reveal real and reciprocal-space patterns. The H-terminated (100) diamond was simulated using a matrix ($M = \begin{bmatrix} 2 & 0 \\ 0 & 1 \end{bmatrix}$) in the *LEEDpat* study, with a set of blue and red spots

corresponding to the two domains in a square lattice. Meanwhile, a matrix ($M = \begin{bmatrix} 1 & 0 \\ 0 & 1 \end{bmatrix}$) with white first-order spots of a hexagon lattice was used to model the (1 × 1) structure for the hydrogenated (111) surface.

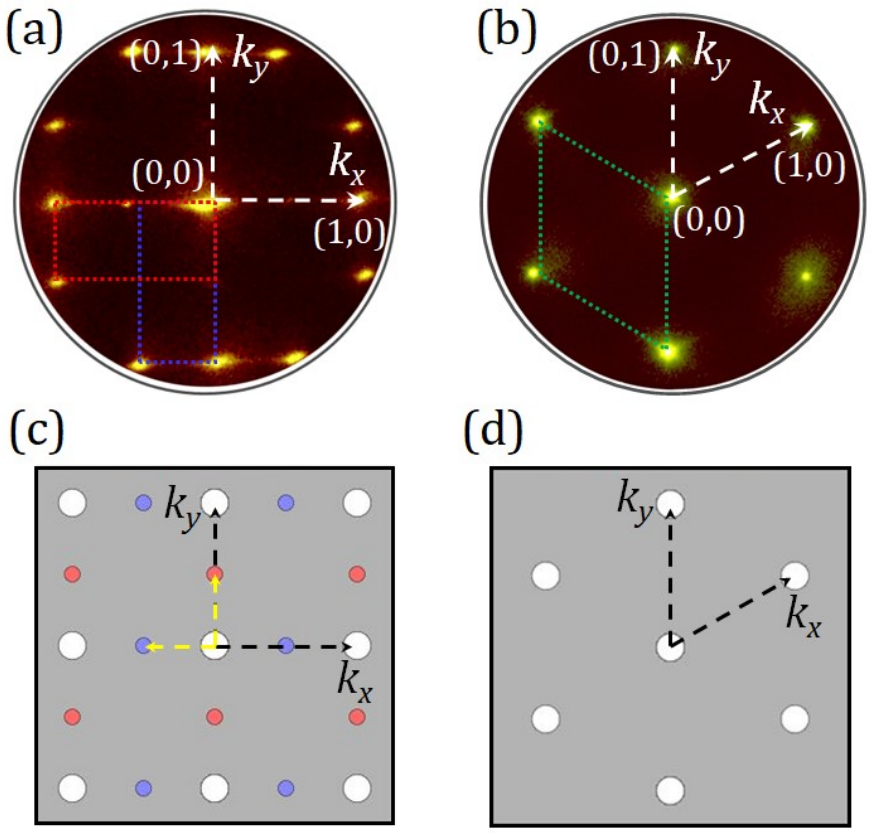

Fig. S2. Experimentally acquired reciprocal-space LEED patterns of the hydrogenated diamond (a) (100) and (b) (111) surfaces. scanned at a beam energy of 100 eV and 150 eV, respectively. White dashed arrows indicate the primitive reciprocal-lattice vectors along the k_x and k_y axes. Blue and red dotted rectangles correspond to two commensurate reconstructions of (2 × 1) and (1 × 2) in panel (a), while in (b), the green dotted rhombus refers to a (1 × 1) diffraction structure. Below is a diagram of the corresponding simulated patterns for the hydrogenated single-crystal diamond (c) (100) and (d) (111) samples, respectively. Blue and red circles in a square lattice are shown for C and H atoms, respectively, whilst white circles refer to the (1 × 1) spots in square and hexagonal lattices.

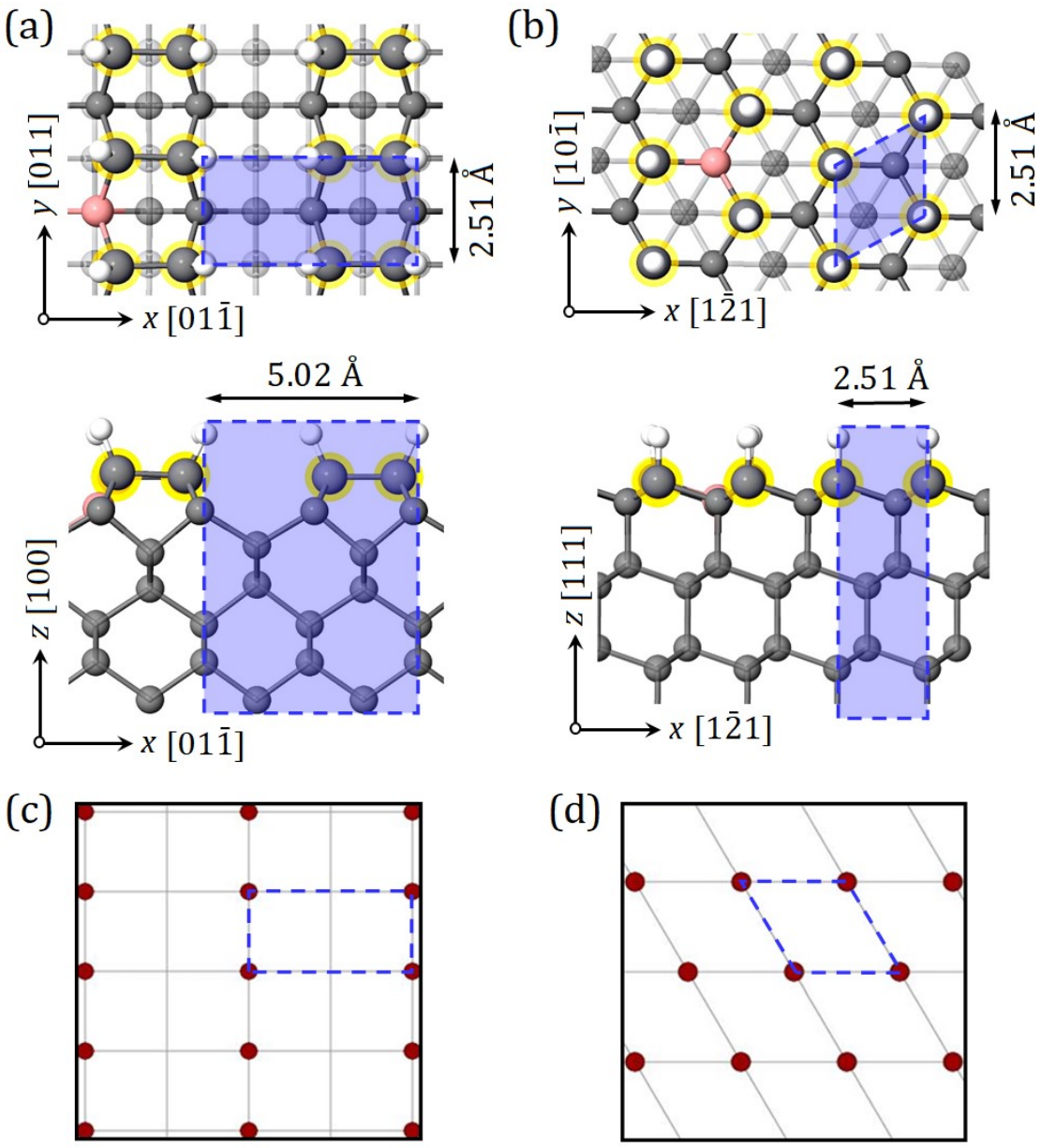

Fig. S3. Top view (above) and side view (below) of the hydrogenated diamond (a) (100) and (b) (111) surfaces, respectively, modelled by DFT calculations. The surface primitive unit cells are indicated by the blue dashed rectangle and rhombohedral shapes, showing (2 × 1) and (1 × 1) structures for the H-terminated (100) and (111) surfaces, respectively. White and grey spheres are H and C atoms, respectively. Dimer and upper-chain C_d atoms are highlighted in yellow. Below is a drawing of a superposition of respective simulated real-space patterns for the hydrogenated diamond (c) (100) and (d) (111) surfaces, respectively. A square grey grid shows the superposition of a real-space lattice. The red circles are associated with the position of individual domains, while the blue dashed rectangle and rhombus show the (2 × 1) and (1 × 1) geometry.

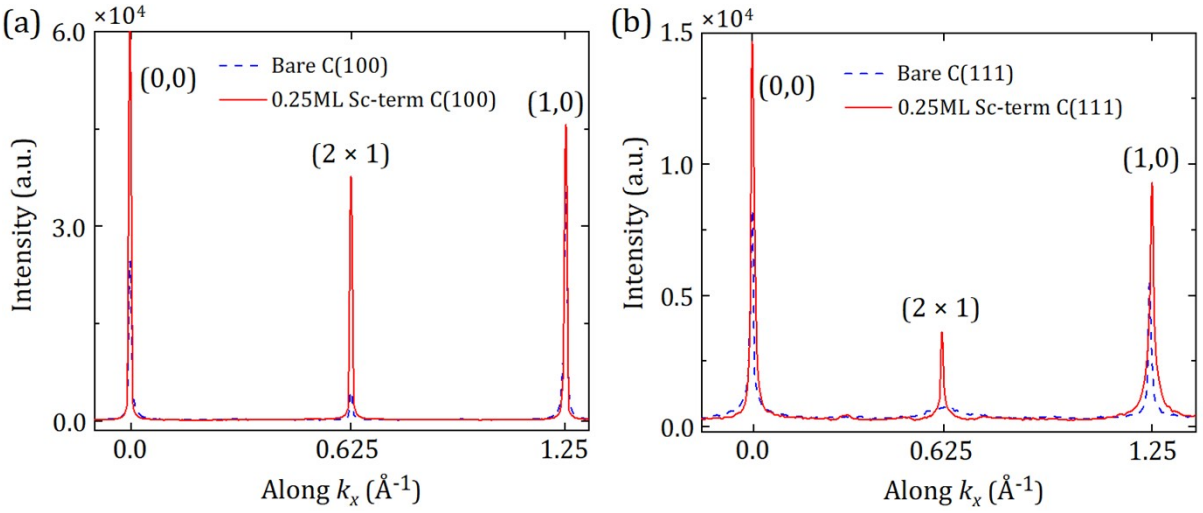

Fig. S4. Spot-profile analysis plots of the bare and 0.25 ML Sc-adsorbed diamond (a) (100) and (b) (111) surfaces along the k_x vector. The signal intensity of the diffraction spots is taken with respect to the background.

S-3. XPS measurements

XPS spectral analysis was performed using the *XPSPEAK41* software (version 4.1) and verified with a well-established fitting program of *CasaXPS* (version 2.3.18)[1] to achieve reproducible GL(*X*) profiles for Gaussian (*Y*%) and Lorentzian (*X*%) sum function with a Shirley background.[2] The best combination of these two functions can vary depending upon the instrumental response (*i.e.* the X-ray line shape of the core hole, pass energy, thermal broadening, *etc.*), providing a better fit for both symmetric and asymmetric peak shapes. For instance, the C 1*s* peak in diamond was fitted better within a GL(20) line shape (*i.e.* Gaussian (80%) and Lorentzian (20%)) (see Table S2). For fitting Sc 2*p* for Sc-terminated bare diamond (100) and (111), GL(46) and GL(42) were found suitable (Table S3). The Sc 2*p* core-level spectra featured Sc $2p_{3/2}$ and Sc $2p_{1/2}$ peaks, which were fitted using an asymmetric peak shape. The area ratio of these two peaks was fixed to be 2:1, consistent with the determined degeneracy ($2j + l$) of the area ratio of individual peaks due to the spin-orbit coupling.[3]

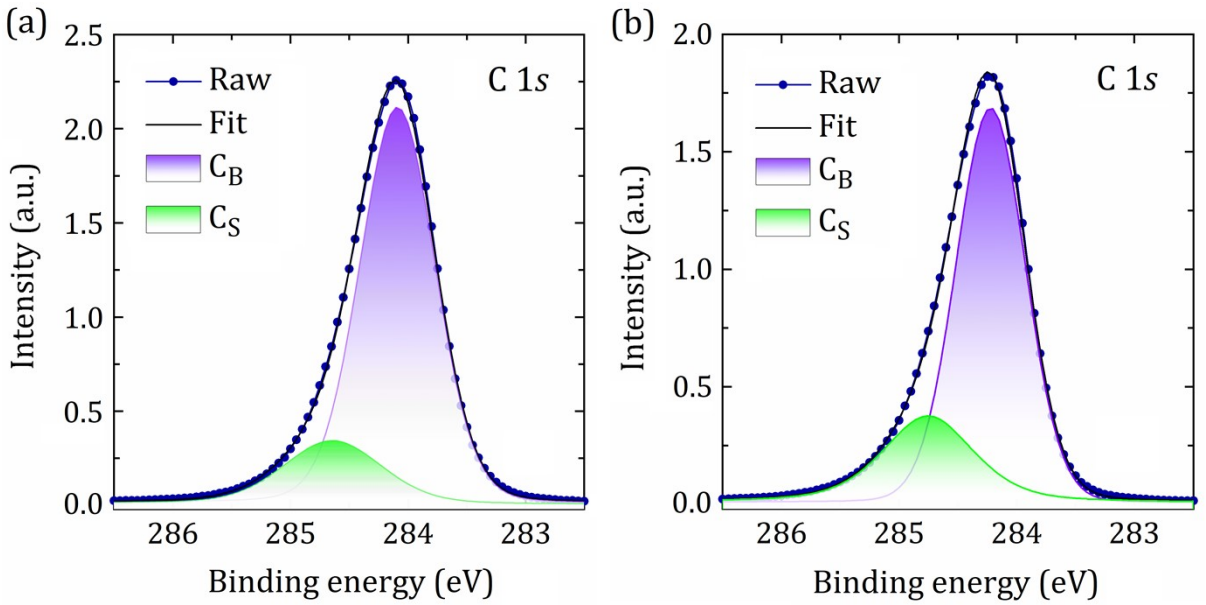

Fig. S5. Core-level spectra of the C 1*s* peak for the H-terminated diamond (a) (100) and (b) (111)-oriented surfaces. C_B and C_S denote bulk and surface carbon components, respectively.

Table S1. Elemental impurity traces in the Sc rod purchased from Testbourne Ltd. Metallic elements were analysed using ICP-OES, while gas elements were detected using the LECO technique. [Data taken from the Testbourne specification data sheet for this Sc rod].

Sc/TREM 99.99%			**TREM 99.5%**		
Elements	**Actual**	**Units**	**Elements**	**Actual**	**Units**
La	5	ppm	Fe	97	ppm
Ce	5	ppm	Si	46	ppm
Pr	1	ppm	Ca	5	ppm
Nd	2.5	ppm	Mg	3	ppm
Sm	0.1	ppm	Al	30	ppm
Er	0.5	ppm	Ni	14	ppm
Eu	0.5	ppm	W	3	ppm
Gd	5.5	ppm	Mo	4	ppm
Tb	2	ppm	Ti	14	ppm
Dy	2	ppm	Ta	340	ppm
Ho	4	ppm	Nb	5	ppm
Tm	0.1	ppm	C	35	ppm
Yb	0.1	ppm	O	122	ppm
Lu	5.5	ppm			
Y	18	ppm			

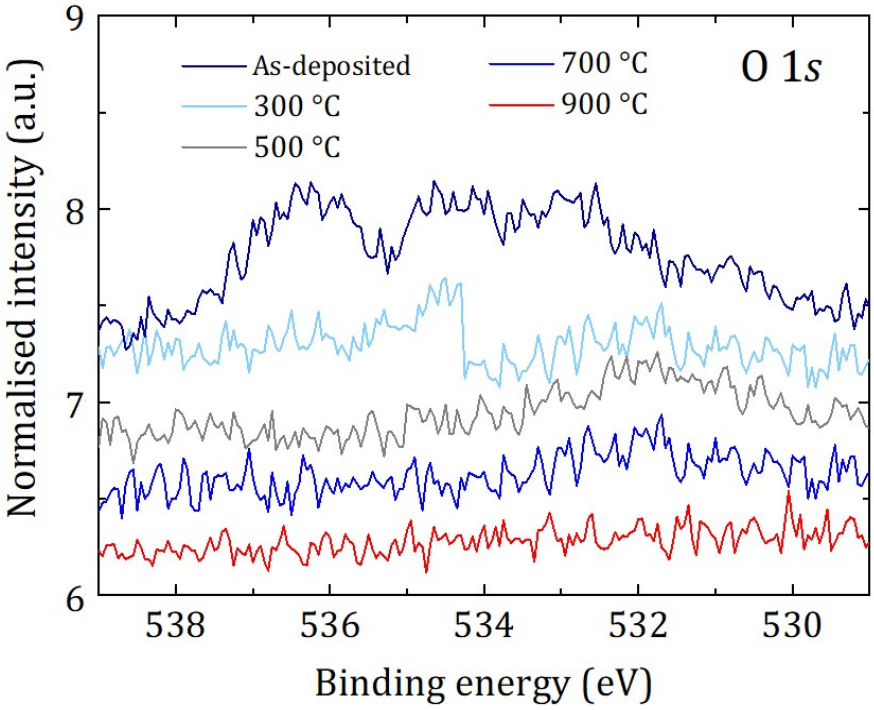

Fig. S6. Core-level spectra of the O 1*s* region for the (100) single-crystal diamond surfaces after each step of the sample preparation.

Table S2. Fitting parameters of the C 1*s* core-level spectra, including binding energy, peak area, fitting profiles (Gaussian (*Y*%)–Lorentzian (*X*%)), actual FWHM, components (C_B and C_S) ratio and splitting distance at various stages of preparation (hydrogenated surface, bare surface, after 0.25 ML Sc deposition and after *in vacuo* annealing at 900 °C) for the (100) and (111) samples.

Sample	C_B / eV	Area / cps	Lorentzian fit / %	Actual FWHM / eV	C_S / eV	Area / cps	Lorentzian fit / %	Actual FWHM / eV	Total Area / cps	C_B/C_S ratio	C_B & C_S splitting
(100) diamond											
H-terminated C_d	284.19	176555.4	15	0.72	284.69	40964.36	28	0.82	217519.76	4.31	0.54
Bare C_d	284.86	183313.1	19	0.82	285.49	46875.15	54	0.86	230188.25	3.91	0.63
As-deposited Sc on	284.76	188552.5	18	0.94	285.45	35057.4	57	0.94	223609.9	5.38	0.69
After 900°C anneal	284.33	196772.2	19	0.83	285.07	37911.44	50	0.83	234683.64	5.19	0.74
(111) diamond											
H-terminated C_d	284.27	128817.5	10	0.69	284.8	39587.14	58	0.81	168404.64	3.25	0.58
Bare C_d	284.94	123215.9	22	0.72	285.47	40162.41	35	0.78	163378.31	3.07	0.53
As-deposited Sc	284.88	124738.3	22	0.8	285.52	30267.02	43	0.86	155005.32	4.12	0.64
After 900°C anneal	284.5	124992.3	19	0.76	285.11	33061.79	56	0.76	158054.09	3.78	0.61

Table S3. Fitting parameters of the Sc 2*p* core-level spectra, including binding energy, peak area, fitting profiles (Gaussian (*Y*%)–Lorentzian (*X*%)), actual FWHM, components (Sc $2p_{3/2}$ and Sc $2p_{1/2}$) ratio and splitting distance at various stages of preparation (after 0.25 ML Sc deposition and after *in vacuo* annealing at 900 °C) for the (100) and (111) samples.

Sample	**Sc $2p_{3/2}$ / eV**	**Area / cps**	**Lorentzian fit / %**	**Actual FWHM / eV**	**Sc $2p_{1/2}$ / eV**	**Area / cps**	**Lorentzian fit / %**	**Actual FWHM / eV**	**Total Area / cps**	**$2p_{3/2}/2p_{1/2}$ ratio**	**$2p_{3/2}$ & $2p_{1/2}$ splitting**
(100) diamond											
As-deposited	398.56	6790.90	25	2.29	403.01	3388.33	36	2.405	10179.23	2.00	4.45
After anneal at 900°C	399.53	7920.99	33	1.98	404.05	4018.72	46	2.226	11939.71	1.97	4.52
(111) diamond											
As-deposited	398.49	7769.57	17	2.04	403.04	3879.88	19	2.32	11649.45	2.00	4.56
After anneal at 900°C	399.17	7758.35	30	1.84	403.66	3955.80	42	2.239	11714.15	1.96	4.49

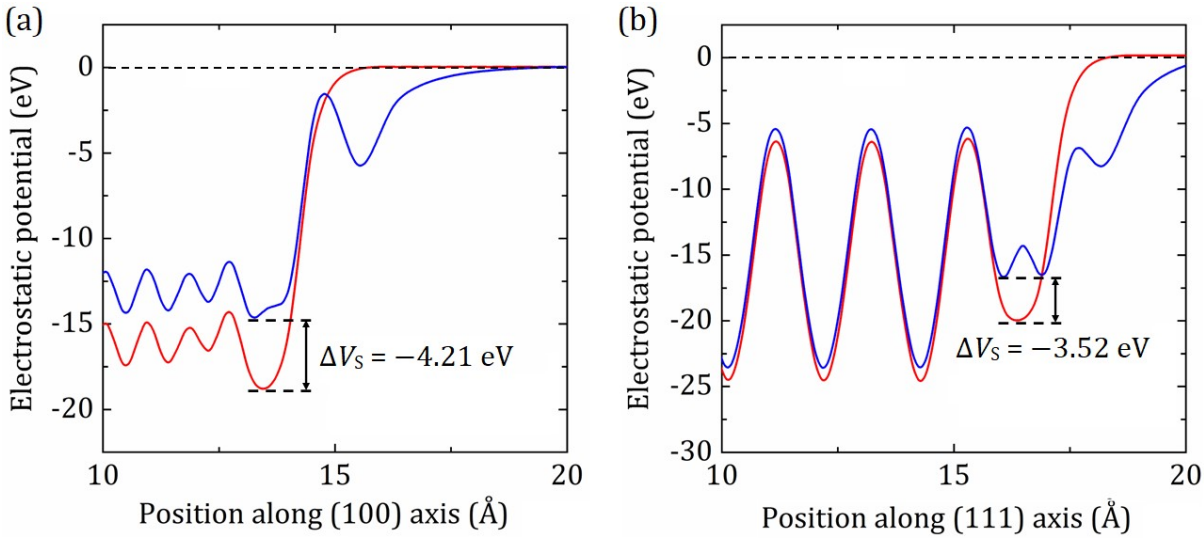

Fig. S7. Plane-averaged electrostatic potential plots for the bare and 0.25 ML Sc-terminated diamond (a) (100) and (b) (111) surfaces, obtained from DFT computation. ΔV_S is the surface potential for the surface C atoms of the bare and 0.25 ML Sc-terminated diamond (100) and (111) surfaces. Blue and red solid lines denote the 0.25 ML Sc-terminated and bare diamond (100) and (111) surfaces, respectively. E_{vac} is set to zero, indicated by the black dotted line.

S-4. UPS and EF-PEEM analysis

S-4.1 H-terminated diamond (100) and (111) surfaces

All the energies in UPS spectra for both hydrogenated single-crystal samples are ascribed relative to the E_F position (Fig. S8). Here and further, the intensity of the spectra are normalised to the "knee" attribute with a BE of ~8.4 eV (or kinetic energy of 12.8 eV), as shown in Fig. S8(b), proposed earlier by O'Donnell *et al.*[4] This attribute usually refers to the lowest energy needed to produce an electron-hole pair,[5, 6] and hence demonstrates the dominant energy-loss step through the transition from pair formation to electron-phonon scattering. Moreover, it is the most suitable normalisation point due to its substantially lower energy than the CBM and the vacuum level because the intensity of surface emissions can be evaluated.

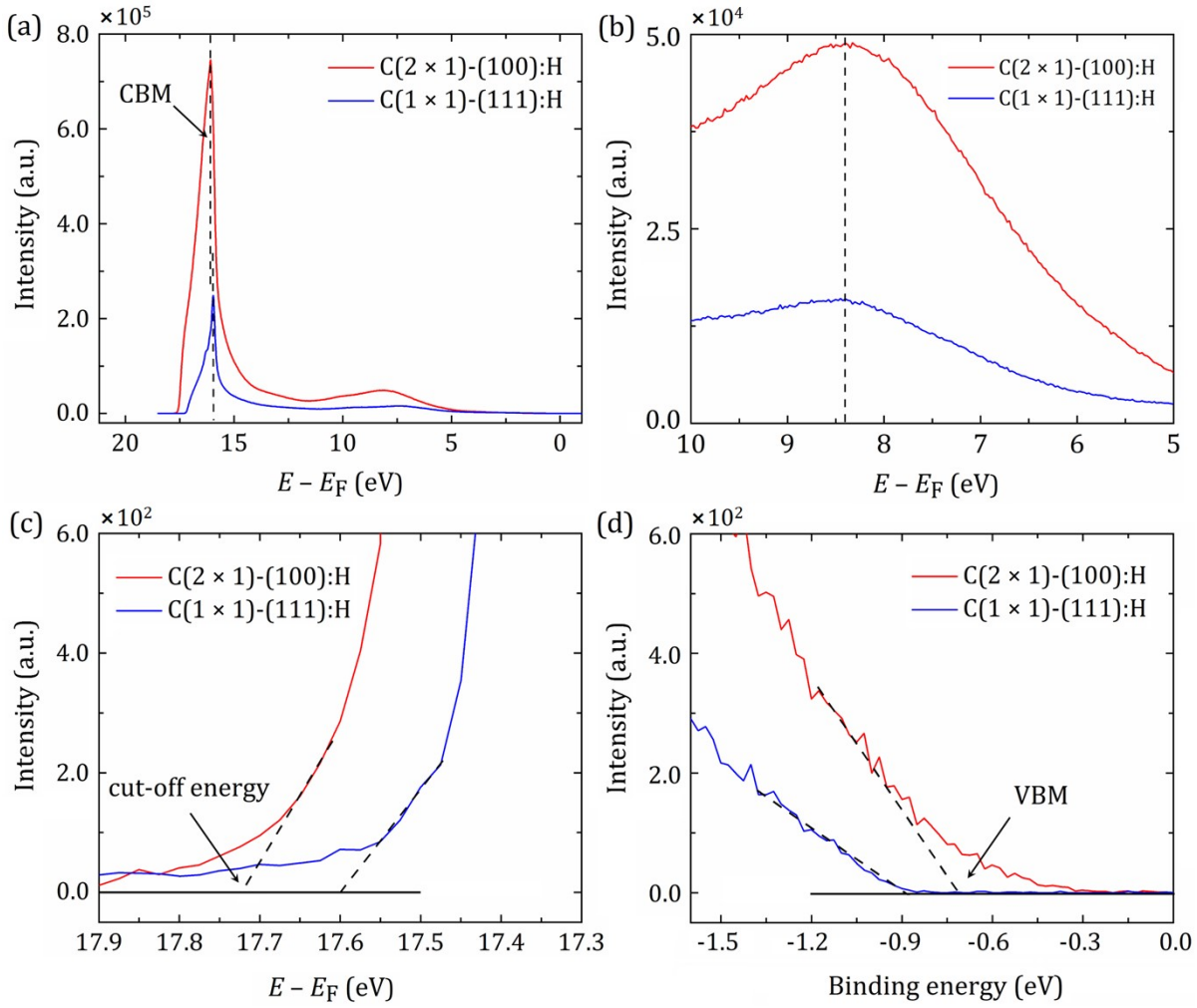

Fig. S8. Region-selected UPS spectra of the hydrogenated diamond (100) and (111) samples illustrating specific panels of interest: (a) the full-scale spectra, (b) the "knee" attribute around 8.4 eV, (c) the cut-off energy and (d) the VBM relative to the Fermi level.

As depicted in Fig. S8(d), the energy level of the VBM relative to E_F is determined by linear extrapolation within the UPS spectrum, while the E_F position is set to zero. Meanwhile, the CBM position relative to E_F can be calculated using this energy difference, as follows:

$$E_{CBM} - E_F = h\nu - (E_F - E_{VBM}) - E_g \quad (1)$$

where $h\nu$ is the UV excitation energy of 21.2 eV and E_g is the experimental band gap of diamond (5.47 eV). The determined positions for both H-terminated (100) and (111) diamond are shown as vertical dashed lines in Fig. S8(a), in reasonable agreement with the highest intensity peak originating from secondary electrons.

Measured EA values for these two hydrogenated (100) and (111) surfaces were in excellent agreement with our DFT simulation and WF maps produced in this work (Fig. S9) and those from previous experimental studies[7-10] (see Tables 1 and 2 in the main text).

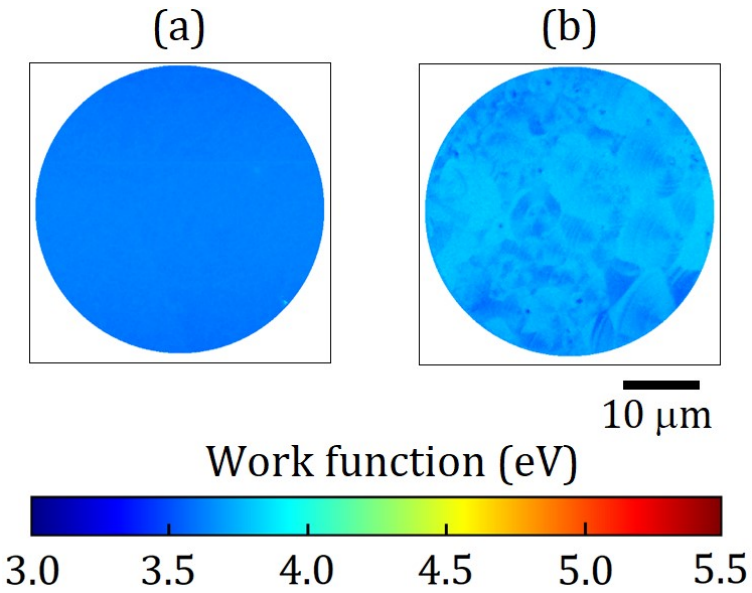

Fig. S9. Colour-coded work-function maps of the hydrogenated diamond (a) (100) and (b) (111) samples observed with the field of view of 37.5 µm.

S-4.2 Sc-terminated diamond (111) surface

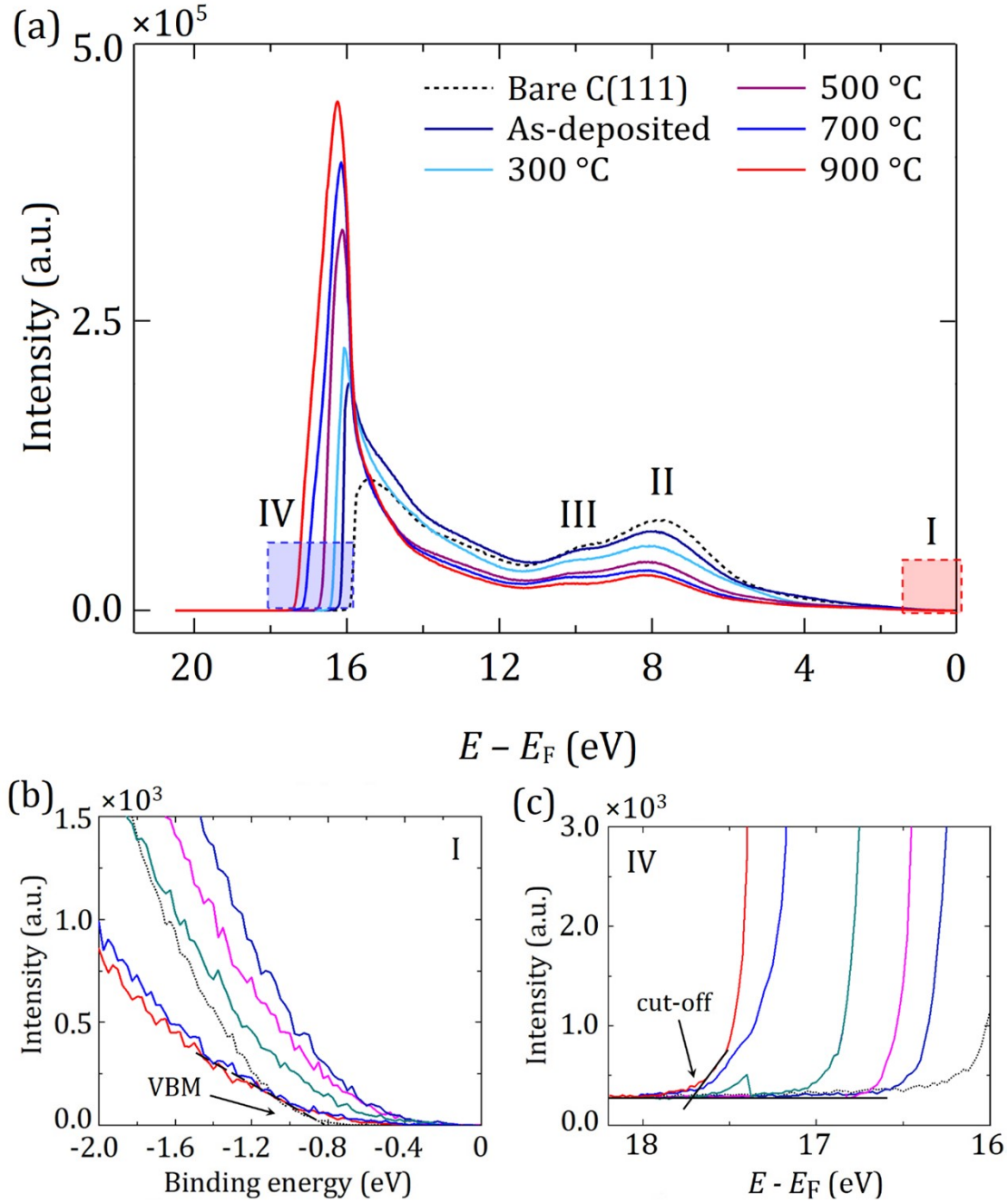

Fig. S10. Region-selected UPS spectra at various stages of the sample preparation (*e.g.* bare diamond, after 0.25 ML Sc deposition and after *in vacuo* annealing stages up to 900 °C) on the diamond (111) surface. (a) UPS spectra labelled with four regions of interest to indicate energy levels. The regions labelled I and IV are depicted in red and blue rectangles, respectively. Corresponding magnified panels define the (b) VBM and (c) cut-off energy relative to the Fermi level, respectively.

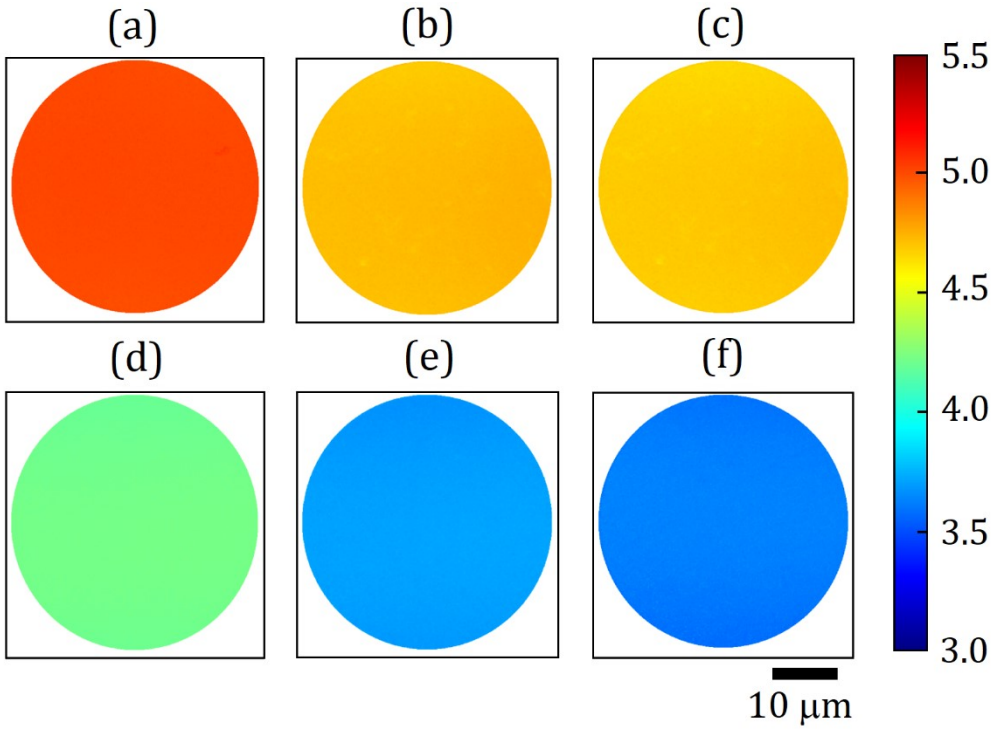

Fig. S11. Colour-coded WF maps at various stages of the sample preparation ((a) 0.25 ML Sc-terminated bare (111) diamond, and annealing at (b) RT, (c) 300 °C, (d) 500 °C, (e) 700 °C and (f) 900 °C). The field of view for all WF maps is 37.5 µm.

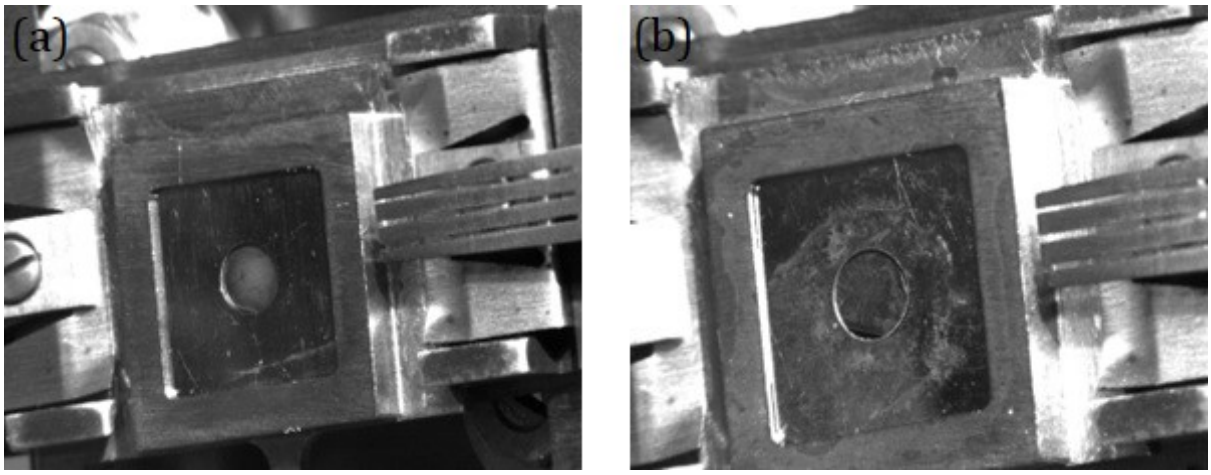

Fig. S12. Photographs of the hydrogenated diamond (a) (100) and (b) (111) samples in the preparation chamber of the NanoESCA facility.

References

1. N. Fairley, V. Fernandez, M. Richard-Plouet, C. Guillot-Deudon, J. Walton, E. Smith, D. Flahaut, M. Greiner, M. Biesinger, S. Tougaard, D. Morgan and J. Baltrusaitis, *Appl. Surf. Sci. Adv*, 2021, **5**, 100112.
2. D. A. Shirley, *Phys. Rev. B*, 1972, **5**, 4709–4714.
3. M. C. Biesinger, L. W. M. Lau, A. R. Gerson and R. S. C. Smart, *Appl. Surf. Sci.*, 2010, **257**, 887–898.
4. K. M. O'Donnell, M. T. Edmonds, J. Ristein, K. J. Rietwyk, A. Tadich, L. Thomsen, C. I. Pakes and L. Ley, *J. Phys.: Condens. Matter*, 2014, **26**, 395008.
5. F. Nava, C. Canali, M. Artuso, E. Gatti, P. F. Manfredi and S. F. Kozlov, *IEEE Trans. Nucl. Sci.*, 1979, **26**, 308–315.
6. B. Ziaja, R. A. London and J. Hajdu, *J. Appl. Phys.*, 2005, **97**, 064905.
7. C. Bandis and B. B. Pate, *Surf. Sci.*, 1996, **350**, 315–321.
8. L. Diederich, O. M. Küttel, P. Aebi and L. Schlapbach, *Surf. Sci.*, 1998, **418**, 219–239.
9. L. Diederich, P. Aebi, O. M. Küttel and L. Schlapbach, *Surf. Sci.*, 1999, **424**, L314–L320.
10. F. Maier, J. Ristein and L. Ley, *Phys. Rev. B*, 2001, **64**, 165411.